Fibroblast-induced mammary epithelial branching depends on fibroblast contractility

Jakub Sumbal[1,2,3], Silvia Fre[2], Zuzana Sumbalova Koledova[1]*

[1]Masaryk University, Faculty of Medicine, Department of Histology and Embryology, Kamenice 3, Brno, 625 00, Czech Republic

[2]Institut Curie, Laboratory of Genetics and Developmental Biology, INSERM U934, CNRS UMR3215, Paris, France

[3]Sorbonne Université, Collège Doctoral, F-75005 Paris, France

ORCID IDs:
JS: 0000-0003-3700-4518;
SF: 0000-0002-7209-7636;
ZSK: 0000-0002-9333-1399.

***Corresponding author and lead contact:**
Zuzana Sumbalova Koledova, PhD.
Department of Histology and Embryology
Faculty of Medicine, Masaryk University
Kamenice 3
625 00 Brno
Czech Republic
koledova@med.muni.cz; Tel: +420 549 49 5049

Total character count: 4631 words (Abstract, Introduction, Results, Discussion, Figure Legends)

Abstract

Epithelial branching morphogenesis is an essential process in living organisms, through which organ-specific epithelial shapes are created. Interactions between epithelial cells and their stromal microenvironment instruct branching morphogenesis but remain incompletely understood. Here we employed fibroblast-organoid or fibroblast-spheroid co-culture systems and time-lapse imaging to reveal that physical contact between fibroblasts and epithelial cells and fibroblast contractility are required to induce mammary epithelial branching. Pharmacological inhibition of ROCK or non-muscle myosin II, or fibroblast-specific knock-out of *Myh9* abrogate fibroblast-induced epithelial branching. Furthermore, fibroblast-induced branching requires epithelial proliferation and is associated with distinctive epithelial patterning of YAP and ERK activity along organoid branches, which is dependent on fibroblast contractility. Together, we identify fibroblast contractility as a novel stromal factor driving mammary epithelial morphogenesis. Our study contributes to comprehensive understanding of overlapping but divergent employment of mechanically active fibroblasts in developmental versus tumorigenic programs.

Key words:
branching morphogenesis, fibroblast, mammary gland, mechanobiology, non-muscle myosin II, organoid, paracrine signaling

Introduction

Efficient formation of large epithelial surfaces in limited organ volumes is achieved through branching morphogenesis (Affolter et al., 2009). The underlying processes of epithelial morphogenesis, including epithelial cell proliferation, migration, intercalation, differentiation, and death, are regulated by both internal genetic programs as well as external cues provided by systemic signals (such as hormones) and local organ-specific microenvironment (Affolter et al., 2009; Goodwin and Nelson, 2020; Wang et al., 2017). The mammary gland is the ideal tissue paradigm for stochastically branching epithelia. Mammary morphogenesis starts in the embryo, but the majority of branch bifurcations and ductal elongation takes place postnatally during puberty. The microenvironment of the mammary epithelium is a dynamic entity that consists of extracellular matrix (ECM) and stromal cells, including fibroblasts. Fibroblasts lay adjacent to the epithelium and have been well recognized as master regulators of mammary epithelial morphogenesis during puberty through production of growth factors (Koledova et al., 2016; Kouros-Mehr and Werb, 2006; Sumbal and Koledova, 2019; Wiseman and Werb, 2002; Zhao et al., 2017) and ECM molecules (Brownfield et al., 2013; Hammer et al., 2017; Jones et al., 2019; Koledova et al., 2016; Nerger et al., 2021; Peuhu et al., 2017; Sumbal and Koledova, 2019; Zhao et al., 2017) necessary for mammary epithelial growth and branching (Sumbal et al., 2020). However, the dynamics of the epithelial-fibroblast interactions during mammary branching morphogenesis as well as whether fibroblasts contribute to shaping of mammary epithelium through additional mechanisms have remained unknown.

Microenvironment of several developing organs has been shown to govern epithelial patterning by dynamic cues of mechanically active cells. Dermal cells in chick skin determine feather buds by mechanical contraction (Shyer et al., 2017), intestinal vilification is dependent on compression by smooth muscle cells (Shyer et al., 2013), and embryonic lung mesenchyme promotes epithelial bifurcation by mechanical forces (Goodwin et al., 2019; Kim et al., 2015; Palmer et al., 2021). However, it has not been elucidated whether the mammary microenvironment contains an instructive component of mechanically active cells as well.

To answer this question, we performed live imaging and functional analysis of co-cultures of primary mammary epithelial organoids with primary mammary fibroblasts. Analogously to primary mammary organoids treated with fibroblast growth factor 2 (FGF2), a well-established model of mammary branching morphogenesis driven by paracrine signals (Ewald et al., 2008), our *in vitro* co-culture model provides a unique window into fibroblast-epithelial interactions during pubertal mammary branching morphogenesis. It enables visualization of stromal fibroblasts during dynamic morphogenetic processes, which are otherwise largely inaccessible *in vivo* due to light-scattering properties of mammary adipose tissue. In this work, we show that physical contact between fibroblasts and epithelial cells, and actomyosin-dependent contractility of fibroblasts are required for branching morphogenesis. Importantly, we demonstrate successful reconstitution of budding morphogenesis by 3D co-culture of contractile fibroblasts in breast cancer spheroids that normally do not form buds. Our results reveal a novel role of fibroblast contractility in driving epithelial branching morphogenesis.

77 ## Results

78 **Fibroblast-induced branching of organoids does not reproduce FGF2-induced budding**

79 To uncover the role of fibroblasts in epithelial morphogenesis, we investigated differences between
80 organoid budding induced solely by paracrine factors (using primary mammary organoids exposed to
81 exogenous FGF2) and organoid branching induced by fibroblasts (using organoids co-cultured with
82 primary mammary fibroblasts in the absence of any exogenous growth factor). Addition of FGF2 or
83 fibroblasts to mammary organoid cultures both induced branching of epithelial organoids (Figure 1A,
84 B, Suppl. Video 1) but examination of the resulting organoid morphogenesis revealed important
85 differences in dynamics and epithelial architecture in the two conditions. First, organoids co-cultured
86 with fibroblasts developed bigger but less numerous branches (Figure 1A, C). Second, they branched
87 half-day to one day earlier than organoids treated with FGF2 (Figure 1A, D) and the branches were
88 developed rapidly, including the development of negative curvature at the root of the branch (Figure
89 1E). Third, while FGF2-induced epithelial branching involved epithelial stratification as previously
90 reported (Ewald et al., 2008), co-culture with fibroblasts did not perturb the epithelial bilayer with its
91 lumen (Figure 1A, G). These results suggest that fibroblasts and exogenous FGF2 drive organoid
92 branching by different mechanisms. While the mechanism of FGF2-induced organoid budding was
93 previously described in detail to begin with epithelial proliferation and stratification (Huebner et al.,
94 2014) followed by budding and ERK-dependent and proliferation-independent bud elongation
95 (Huebner et al., 2016) , how fibroblasts induce organoid branching remains unanswered (Figure 1F).

96 **Endogenous paracrine signals are not sufficient to induce organoid branching in co-cultures**

97 The ability of exogenous FGF2 to promote organoid budding (Ewald et al., 2008) (Figure 1A) well
98 demonstrates the importance of paracrine signals for epithelial branching, although FGF2 amount used
99 in *in vitro* branching assays likely exceeds physiological values *in vivo*. Therefore we sought to
100 determine, whether endogenous FGFs or other paracrine signals produced by fibroblasts in co-cultures
101 (Koledova et al., 2016, 1; Sumbal and Koledova, 2019) are sufficient to drive organoid branching. First
102 to test the involvement of FGF signaling, we inhibited either FGF receptors (FGFRs) using SU5402, or
103 ERK, a common signaling node of all receptor tyrosine kinases using U0126. As expected, both
104 inhibitors abolished branching induced by exogenous FGF2 (Figure 2A, B). However, in the co-cultures
105 with fibroblasts, the same concentration of inhibitors did not abolish branching, albeit slightly reduced
106 organoid growth (Figure 2A, B), suggesting that paracrine signaling via FGFR-ERK pathway is not the
107 only mechanism driving organoid branching.

108 To probe the involvement of other paracrine signaling in fibroblast-induced organoid branching,
109 namely to test if fibroblast paracrine signaling alone is sufficient to induce organoid branching, or if
110 other mechanisms involving fibroblast-epithelial proximity or contact are involved, we performed an
111 array of different types of organoid (co-)culture set-ups (Figure 2D, top). When we provided
112 unidirectional fibroblasts-to-epithelium paracrine signals by culture of organoids in fibroblast-
113 conditioned medium, no organoid branching was observed (Figure 2C, D). When we allowed
114 bidirectional paracrine signals by co-culture of organoids with fibroblasts in the same well but the
115 organoids and fibroblasts were separated by a transwell membrane or by a thick layer of Matrigel, no
116 organoid branching was observed either (Figure 2C, D). However, when we allowed both paracrine
117 signals and physical contact between organoid and fibroblasts by co-culturing them together either
118 dispersed in Matrigel or as aggregates of fibroblasts on top of organoids embedded in Matrigel, we
119 observed organoid branching (Figure 2C-E). These results demonstrated an essential requirement of

120 fibroblast-epithelium contact for fibroblast-induced organoid branching thus revealing that fibroblast-
121 secreted paracrine factors are not sufficient to initiate branching.

122 **MCF7-ras spheroids recapitulate fibroblast-induced branching of organoids**

123 To further test the requirement of fibroblast-epithelium contact for fibroblast-induced epithelial
124 branching, we developed a simpler co-culture system, where mammary fibroblasts were co-cultured
125 with MCF7-ras breast cancer cell line spheroids (Figure 2F) instead of organoids from normal mammary
126 epithelium. The advantage of MCF7-ras spheroids is that the spheroids grow constantly due to
127 constitutively active RAS kinase and unlike normal epithelium they do not respond to exogenous FGF2
128 (Figure 2G) or EGF (Suppl. Figure 1A) by branching. We found that similarly to normal epithelium,
129 MCF7-ras spheroids remained round in fibroblast co-cultures, which did not allow physical contact with
130 fibroblasts, but developed numerous buds when physical contact with fibroblasts was allowed (Figure
131 2H; Suppl. Figure 1B). These results demonstrated that fibroblasts are able to promote epithelial
132 budding even in a system that is morphogenetically unresponsive to paracrine signals.

133 **Fibroblasts form physical contact with organoids**

134 To gain more insights into the mechanism of fibroblast-induced organoid branching, we examined
135 organoid branching in the co-cultures in higher resolution. First, we performed a co-culture experiment
136 with organoids labeled by mTomato and GFP-tagged fibroblasts. The time-lapse movies unveiled that
137 fibroblasts came in close contact with the epithelium early during the co-culture and remained there
138 during branching (Figure 3A, Suppl. Video 2). On the branched organoids, fibroblasts were exclusively
139 located around the necks of the nascent branches and sat directly in contact with the epithelium
140 (Figure 3B). Immunofluorescence staining of epithelial markers revealed that fibroblasts formed
141 contacts with KRT5 positive myoepithelial cells (Figure 3C, Suppl. Video 3). Transmission electron
142 microscopy of the co-cultures confirmed the close proximity between the fibroblasts and the
143 epithelium, with a thin layer of ECM in between (Figure 3D). Using immunostaining we detected
144 laminin α5, a basal membrane component, between organoid and adjacent fibroblast (Figure 3E, F).
145 These data suggest that fibroblasts form contacts with epithelium via ECM.

146 **Fibroblast-induced epithelial branching depends on fibroblast contractility**

147 Based on observations from the time-lapse videos of organoids branched by fibroblasts (Suppl. Videos
148 1 and 2) we hypothesized that fibroblasts could constrict epithelium, folding it into branches.
149 Immunofluorescence investigation of fibroblast-branched organoids revealed that fibroblasts in
150 contact with the organoid formed a cellular loop, encircling the branch neck (Figure 4A), and contained
151 F-actin cables oriented mostly perpendicularly to the branch longitudinal axis (Figure 4A). Moreover,
152 the fibroblasts expressed phosphorylated myosin light chain 2 (P-MLC2), a marker of active non-muscle
153 myosin II (Figure 4B). Therefore, we examined the involvement of fibroblast contractility in fibroblast-
154 induced organoid branching using small molecule inhibitors of non-muscle myosin II (blebbistatin) or
155 ROCK1/2 (Y27632), two major nodes of cell contractility. The contractility inhibitors abrogated
156 branching in co-cultures but did not inhibit organoid budding induced by exogenous FGF2 (Figure 4C,
157 D; ROCK inhibition in FGF2-induced organoids even led to hyperbranched phenotype as previously
158 described (Ewald et al., 2008)). Similarly, in the MCF7-ras spheroid co-culture model, spheroid budding
159 was inhibited by addition of contractility inhibitors (Suppl. Figure 2A-D).

160 Because exogeneous treatment with pharmacological inhibitors in the culture medium affects both
161 epithelial cells and fibroblasts, we genetically targeted exclusively in fibroblasts the contractility
162 machinery gene myosin heavy chain 9 (*Myh9*), one of the two non-muscle myosin II heavy chain genes

163 expressed in mammary fibroblasts (Suppl. Figure 3A, B). Both siRNA-mediated *Myh9* knock-down in
164 wild-type fibroblasts and adenoviral Cre-mediated knock-out in *Myh9*$^{fl/fl}$ fibroblasts led to a decrease
165 of organoid branching in co-cultures (Figure 4E, F; Suppl. Figure 4A-E; Suppl. Videos 4 and 5). These
166 results demonstrate that fibroblast contractility is required for organoid branching in co-cultures.

167 **Fibroblast-induced epithelial branching requires epithelial proliferation**

168 Mesenchymal cell tension coupled with expansion of underlying epithelium has been recently shown
169 to cause corrugation of lung in lizard (Palmer et al., 2021). Similarly, contractile fibroblasts wrapped in
170 loops around an expanding epithelial organoid/spheroid could be causing the branched outcome in
171 our co-culture models. One of the common mechanisms of epithelial expansion is cell division;
172 therefore, we characterized proliferation in the organoid-fibroblast co-culture model by both
173 immunodetection for proliferation marker protein KI67 (Figure 5A) and by EdU incorporation (Figure
174 5B). EdU incorporation revealed proliferation also in fibroblast-free culture, suggesting that insulin-
175 containing basal medium promotes cell division in organoids (Suppl. Figure 5A-C). However, we have
176 observed regionalization of proliferation in organoids co-cultured with fibroblast with the most
177 proliferative cells present in the neck of the branch and less at the branch tip (Figure 5C).

178 To test whether epithelial proliferation (and thus expansion) plays a role in organoid branching in
179 co-cultures, we inhibited cell proliferation using aphidicolin (DNA polymerase inhibitor), upon which
180 we observed a severe defect in organoid branching (Figure 5D-F). To test for the possibility that the
181 observed effect could be caused by inhibition of fibroblast proliferation, we performed the experiment
182 also with fibroblasts pretreated with mitomycin C, an irreversible DNA synthesis blocker (Figure 5D).
183 The pretreatment of fibroblast with mitomycin C had no effect on the result (Figure 5D-F),
184 demonstrating that fibroblast proliferation is dispensable while epithelial proliferation is necessary for
185 organoid branching in co-cultures. In concordance with the results from organoid co-cultures, in the
186 MCF7-ras spheroid co-culture model the blockage of spheroid proliferation by mitomycin C
187 pretreatment of spheroids decreased spheroid size expansion and dramatically decreased branching
188 of the MCF7-ras spheroids (Suppl. Figure 6A, B).

189 The regionalization of epithelial proliferation (Figure 5C) suggested an epithelial signaling response to
190 fibroblast contact. Therefore, we examined the subcellular localization of yes associated protein (YAP),
191 a mechano-sensor that in a resting cell resides in the cytoplasm but translocates to the nucleus upon
192 mechanical stress (Panciera et al., 2017), and phosphorylated (active) ERK (P-ERK), the regulator of
193 mammary epithelial branching (Ender et al., 2022; Huebner et al., 2016) as two candidates. We found
194 that YAP specifically accumulated in the nuclei of epithelial cells in the neck region of epithelial branch
195 (Figure 5G), indicating that the contact with contractile fibroblasts can be sensed by the underlying
196 epithelial cells as a mechanical stress. Moreover, we found that P-ERK was localized inversely to YAP
197 (Figure 5G, H). To test the effect of fibroblast contractility on epithelial YAP end ERK signaling, we
198 stained YAP and P-ERK also in co-cultures with *Myh9* knockout fibroblasts. Knockout of *Myh9* in
199 fibroblasts prevented YAP and P-ERK gradient formation (Figure 5I), indicating that contact with
200 contractile fibroblasts regulate YAP and P-ERK epithelial distribution. Together, our data suggest that
201 mechanical constriction by contractile fibroblasts is actively sensed by mammary epithelial cells,
202 similarly to what was recently observed in intestinal organoids (Pérez-González et al., 2021) with the
203 interesting difference that in our heterotypic co-culture system, the curvature of the epithelium
204 depends on physical contact with contractile stromal cells.

205 ## Discussion

206 Mechanical forces are an integral part and a driving factor of tissue morphogenesis. However, the
207 sources of mechanical forces in different tissues are still unclear and little is understood of how force
208 sensing is translated into cell fate during organ formation. Our work reveals the critical role of
209 fibroblast-derived mechanical forces in regulation of mammary epithelial branching morphogenesis. It
210 demonstrates that mammary fibroblasts generate mechanical forces via their actomyosin apparatus
211 and transmit them to the epithelium, which leads to epithelial deformation and patterning of epithelial
212 intracellular signaling, resulting in epithelial folding into branched structures.

213 *Fibroblast-generated mechanical forces as part of complex tissue mechanics*

214 The role of intraepithelial forces in morphogenetic processes involving tissue folding, such as
215 gastrulation, tubulogenesis, or buckling has been long recognized and intensively studied (Heisenberg
216 and Bellaïche, 2013). Similarly, the instructive role of mechanical properties and 3D organization of the
217 ECM in determination of cell fate and behavior during organ formation, including mammary epithelial
218 branching morphogenesis, has been well established (Bonnans et al., 2014; Brownfield et al., 2013;
219 Nguyen-Ngoc and Ewald, 2013). However, the evidence for regulation of epithelial morphogenesis by
220 mechanical stimuli from mesenchymal cells was discovered only recently and has been scarce, limited
221 to the morphogenesis of feather buds in chick skin by mechanically active dermal cells (Shyer et al.,
222 2017), gut villification (Shyer et al., 2013) and lung epithelial bifurcation and alveologenesis induced
223 by smooth muscle cells or myofibroblasts (Goodwin et al., 2019; Kim et al., 2015; Li et al., 2020a;
224 Palmer et al., 2021).

225 *The mechanism of fibroblast-induced mammary morphogenesis: connection to ECM remodeling*

226 It was previously proposed that mechanical forces generated by mesenchymal/stromal cells regulate
227 epithelial morphogenesis indirectly via changes of ECM mechanics, including collagen I remodeling in
228 embryonic gut (Hughes et al., 2018) and postnatal mammary gland (Koledova et al., 2016; Peuhu et
229 al., 2017; Sumbal et al., 2020), or elastin deposition in lung (Li et al., 2018). However, while not
230 excluding contribution of such mechanism to mammary epithelial branching *in vivo*, our investigations
231 *in vitro* in organoid-fibroblast co-cultures devoid of collagen I demonstrate that collagen I fibers are
232 not required for induction of epithelial folding by fibroblast contractility. Mammary fibroblasts form
233 direct, highly dynamic contacts with mammary epithelial cells and induce a mechanosensitive response
234 in the epithelium, resulting in patterning of key morphogenetic regulators YAP and ERK. The direct
235 contact between mammary fibroblasts and epithelial cells *in vivo* could be enabled by immature, thin
236 basement membrane of terminal end buds (Silberstein and Daniel, 1982), the highly proliferative
237 epithelial structures, which drive postnatal mammary branching morphogenesis, and active
238 remodeling of ECM by matrix metalloproteinases produced by both epithelial cells and fibroblasts
239 (Feinberg et al., 2018), which is essential for mammary branching morphogenesis (Fata et al., 2004;
240 Feinberg et al., 2018). Our work does not exclude the importance of ECM remodeling by fibroblast
241 mechanical forces in epithelial branching. We speculate that *in vivo* the highly dynamic mechanically
242 active fibroblasts could initiate formation of epithelial clefts and further reinforce them by subsequent
243 deposition and remodeling of ECM.

244 *The mechanism of fibroblast-induced mammary morphogenesis: requirement of paracrine signaling*

245 Importantly, our results do not rule out the importance of fibroblast-secreted factors in mammary
246 epithelial morphogenesis. However, we demonstrate that paracrine signals are not sufficient to drive
247 organoid branching in the 3D *in vitro* cultures of organoids with fibroblasts without addition of any

248 branching-inducing growth factors and show the importance of fibroblast-epithelium contact, so short-
249 distance paracrine or juxtacrine signals could be important in the process. Several growth factors,
250 including FGF2, FGF7, EGF or TGFα can induce organoid branching in the absence of fibroblasts when
251 added to the medium in nanomolar concentrations (Sternlicht et al., 2005). However, the evidence for
252 requirement of those growth factors' expression in mammary fibroblasts for mammary epithelial
253 branching *in vivo* is missing.

254 *The mechanism of fibroblast-induced mammary morphogenesis: epithelial response*

255 Our work reveals that mechanical strain imposed on mammary epithelial cells by fibroblasts results in
256 epithelial folding with negative curvature in the epithelial-fibroblast contact points, which show low
257 ERK activity, and positive curvature in the branch tips, which show high ERK activity. This distribution
258 of active ERK is in line with the role of ERK in mammary branch elongation (Huebner et al., 2016) and
259 with a recent study indicating that ERK is specifically activated in epithelia with a positive curvature in
260 the developing lung (Hirashima and Matsuda, 2021). While the mechanisms of epithelial folding, ERK
261 spatial pattern formation, and their interplay during fibroblast-induced mammary epithelial
262 morphogenesis remain to be investigated, they could include ERK-mediated mechanochemical waves
263 as described during 2D collective cell migration (Hino et al., 2020).

264 Importantly, the direct interactions between mammary epithelium (including both organoids from
265 normal epithelium and spheroids from breast cancer cells) and fibroblasts do not lead to invasive
266 dissemination of epithelial cells, unlike in co-cultures of squamous cell carcinoma with cancer-
267 associated fibroblasts (CAFs) (Labernadie et al., 2017). Interestingly, a recent study described
268 mechanical compression of intestinal tumors by CAFs forming a mechanically active tumor capsule
269 (Barbazan et al., 2021), providing further evidence for context-dependent employment of fibroblast-
270 derived mechanical forces in tissue morphogenesis and tumorigenesis.

271 *Fibroblasts as central regulators of epithelial morphogenesis and homeostasis: evidence for*
272 *mechanically active fibroblasts in vivo*

273 Fibroblasts accompany mammary epithelial cells from early development through homeostasis to
274 aging and disease and employ different functions to meet epithelial needs (Sumbal et al., 2020). The
275 multiple fibroblast functions are facilitated by fibroblast heterogeneity, which has only recently begun
276 to be resolved using single-cell RNA sequencing approaches (Li et al., 2020b; Yoshitake et al., 2022).
277 These studies confirmed well-established fibroblast roles in epithelial development and tissue
278 homeostasis via production of paracrine signals and ECM, and fibroblast roles in regulation of immune
279 landscape of the mammary gland. Though they did not detect mechanically active fibroblasts.
280 However, these studies included only adult and aged mammary glands and omitted puberty, the stage
281 of active mammary epithelial branching morphogenesis, thus the *in vivo* existence of mechanically
282 active mammary fibroblasts in normal mammary gland requires further investigation. The presence
283 and function of mechanically active fibroblasts (contractile fibroblasts expressing αSMA,
284 myofibroblasts) has been well documented in other developing organs (Li et al., 2018) and in multiple
285 tumor types, including mammary carcinomas (Costa et al., 2018; Sahai et al., 2020).

286 In conclusion, we find that fibroblasts drive branching morphogenesis of the mammary gland by
287 exerting mechanical forces on epithelial cells. It is conceivable that such conserved mechanism could
288 be used to regulate morphogenesis of other branched organs, providing a comprehensive
289 understanding of overlapping but divergent employment of mechanically active fibroblasts in
290 developmental versus tumorigenic programs.

291 ## Materials and Methods

292 **Animals**

293 All procedures involving animals were performed under the approval of the Ministry of Agriculture of
294 the Czech Republic (license # MSMT-9232/2020-2), supervised by the Expert Committee for Laboratory
295 Animal Welfare of the Faculty of Medicine, Masaryk University, at the Laboratory Animal Breeding and
296 Experimental Facility of the Faculty of Medicine, Masaryk University (facility license #58013/2017-
297 MZE-17214), or under the approval of the ethics committee of the Institut Curie and the French
298 Ministry of Research (reference #34364-202112151422480) in the Animal Facility of Institut Curie
299 (facility license #C75–05–18). ICR mice were obtained from the Laboratory Animal Breeding and
300 Experimental Facility of the Faculty of Medicine, Masaryk University. *R26-mT/mG* (Muzumdar et al.,
301 2007) and *Acta2-CreERT2* mice (Wendling et al., 2009) were acquired from the Jackson Laboratories.
302 LifeAct-GFP mice (Riedl et al., 2010) were created by Wedlich-Söldner team, *Myh9*$^{fl/fl}$ mice (Conti et al.,
303 2004) were kindly provided by Dr. Sara Wickström. Transgenic animals were maintained on a C57/BL6
304 background. Experimental animals were obtained by breeding of the parental strains, the genotypes
305 were determined by genotyping. The mice were housed in individually ventilated or open cages, all
306 with ambient temperature of 22°C, a 12 h:12 h light:dark cycle, and food and water *ad libitum*. Female
307 6-8 weeks old virgin mice were used in the experiments. Mice were euthanized by cervical dislocation
308 and mammary gland tissues were collected immediately.

309 **Primary mammary organoid and fibroblast isolation and culture**

310 Primary mammary fibroblasts and organoids were isolated from 6-8 weeks old female virgin mice (ICR,
311 unless otherwise specified) as previously described (Koledova, 2017). The mammary glands were
312 chopped and partially digested in a solution of collagenase and trypsin [2 mg/ml collagenase A, 2
313 mg/ml trypsin, 5 µg/ml insulin, 50 µg/ml gentamicin (all Merck), 5% fetal bovine serum (FBS;
314 Hyclone/GE Healthcare) in DMEM/F12 (Thermo Fisher Scientific)] for 30 min at 37°C. Resulting tissue
315 suspension was treated with DNase I (20 U/ml; Merck) and submitted to five rounds of differential
316 centrifugation (450 × g for 10 s) to separate epithelial (organoid) and stromal fractions. The organoids
317 were resuspended in basal organoid medium [1× ITS (10 µg/ml insulin, 5.5 µg/ml transferrin, 6.7 ng/ml
318 sodium selenite), 100 U/ml of penicillin, and 100 µg/ml of streptomycin in DMEM/F12] and kept on ice
319 until co-culture setup. The cells the from stromal fraction were pelleted by centrifugation, suspended
320 in fibroblast cultivation medium (10% FBS, 1× ITS, 100 U/ml of penicillin, and 100 µg/ml of
321 streptomycin in DMEM) and incubated on cell culture dishes at 37°C, 5% CO_2 for 30 min. Afterwards
322 the unattached (non-fibroblast) cells were washed away, the cell culture dishes were washed with PBS
323 and fresh fibroblast medium was provided for the cells. The cells were cultured until about 80%
324 confluence. During the first cell subculture by trypsinization, a second round of selection by differential
325 attachment was performed, when the cells were allowed to attach only for 15 min at 37°C and 5% CO_2.
326 The fibroblasts were expanded and used for the experiments until passage 5.

327 To inhibit fibroblast proliferation for specific assays, the fibroblasts were treated with 10 µg/ml
328 mitomycin C in fibroblast medium for 3 h at 37°C, 5% CO_2. Afterwards the fibroblasts were washed
329 three times with PBS and one time with basal organoid medium, trypsinized and used to set up co-
330 cultures.

331 To prepare fibroblast-conditioned medium, the fibroblasts were seeded in cell culture dishes in
332 fibroblast medium and the next day, the cells were washed three times with PBS and incubated with
333 basal organoid medium for 24 h. Afterwards the medium was collected from the dishes, sterile-filtered

334 through a 0.22 µm filter, and used immediately in the experiment, or aliquoted, stored at -20°C and
335 used within 5 days of conditioned medium preparation.

336 **3D culture of mammary organoids and fibroblasts**

337 3D culture of mammary organoids and fibroblasts was performed as previously described (Koledova
338 and Lu, 2017). Freshly isolated mammary organoids were embedded in Matrigel either alone (300
339 organoids in 45 µl of Matrigel per well) or with 5×10^4 mammary fibroblasts per well and plated in
340 domes in 24-well plates. For transwell experiments, organoids were plated in domes in the transwell
341 (8 µm pore size, Falcon-Corning), fibroblasts were plated in lower chamber. After setting the gel for
342 45-60 min at 37°C, the cultures were overlaid with basal organoid medium (1× ITS, 100 U/ml of
343 penicillin, and 100 µg/ml of streptomycin in DMEM/F12), not supplemented or supplemented with
344 growth factors [2.5 nM FGF2 (Enantis)] or small molecule inhibitors (Suppl. Table 1) according to the
345 experiment. The cultures were incubated in humidified atmosphere of 5% CO_2 at 37°C on Olympus
346 IX81 microscope equipped with Hamamatsu camera and CellR system for time-lapse imaging. The
347 organoids/co-cultures were photographed every 60 min for 5 days with manual refocusing every day
348 (high-detail imaging) or photographed only once per day for 5 days (low-detail imaging). The images
349 were exported and analyzed using Image J. Organoid branching was evaluated from videos and it was
350 defined as formation of a new bud/branch from the organoid. Organoids that fused with another
351 organoid or collapsed after attachment to the bottom of the dish were excluded from the
352 quantification.

353 For fluorescent time-lapse imaging, organoids were isolated from *R26-mT/mG* mammary
354 glands on day of the experiment. Fibroblasts were isolated from *Acta2-CreERT2;mT/mG* mice, cultured
355 to passage 2-3 and induced *in vitro* by 0.5 mM 4-OH-tamoxifen (Sigma) treatment for 4 days prior
356 trypsinization and experimental use. Before experiment, the GFP fluorescence of fibroblasts was
357 assessed using a microscope and when it was > 95%, the cells were used for co-culture. Co-cultures
358 were seeded on coverslip-bottom 24-well plate (IBIDI) and imaged on Cell Discoverer 7 equipped with
359 PLAN-APOCHROMAT 20x/0.95 autocorr with 0.5× magnification lens. GFP was imaged with 470/40
360 excitation, 525/50 emission, tdTomato was imaged with 545/25 excitation, 605/70 emission filter (all
361 Zeiss). The samples were incubated in a humidified atmosphere of 5% CO_2 at 37°C during the imaging.

362 **3D culture of spheroids and fibroblasts**

363 MCF7-ras cells (kindly provided by Dr. Ula Polanska) were expanded in DMEM/F12 supplemented with
364 10% FBS, 100 U/ml of penicillin, and 100 µg/ml of streptomycin and incubated in non-adherent
365 PolyHEMA-coated dish overnight to form spheroids. Next day, the spheroids were embedded either
366 alone (200 spheroids in 45 µl of Matrigel per well) or with 5×10^4 mammary fibroblasts per well and
367 plated in domes in 24-well plates. After setting the gel for 45-60 min at 37°C, the cultures were overlaid
368 with basal organoid medium, supplemented with growth factors [2.5 nM FGF2 (Enantis) or EGF
369 (Peprotech)] small molecule inhibitors (Suppl. Table 1) according to the experiment. The (co-)cultures
370 were incubated in a humidified atmosphere of 5% CO_2 at 37°C on Olympus IX81 microscope equipped
371 with Hamamatsu camera and CellR system for time-lapse imaging and photographed every 60 min for
372 5 days with manual refocusing every day (high-detail imaging) or photographed only once per day for
373 5 days (low-detail imaging). The images were exported and analyzed using Image J. Spheroid budding
374 was evaluated from the videos and it was defined as formation of a new bud from the spheroid.
375 Spheroids that fused with other spheroids were excluded from the quantification.

376 **Knockdown and knockout of *Myh9* in mammary fibroblasts**

377 For *Myh9* knockdown, the pre-designed Silencer Select siRNAs against *Myh9* (IDs s70267 and s70268,
378 Myh9si#1 and Myh9si#2, respectively) and the scrambled negative control siRNA (Silencer Select
379 negative control or Stealth negative control siRNA), all from Thermo Fisher Scientific, were transfected
380 into wild type (ICR) fibroblasts with Lipofectamine 3000 Reagent (Thermo Fisher Scientific) according
381 to manufacturer's instructions at 20 nM siRNA. For *Myh9* knockout, *Myh9*$^{fl/fl}$ fibroblasts were
382 transduced with adenoviruses Adeno-Cre-GFP (Ad-Cre-GFP) or Adeno-GFP (Ad-GFP) from Vector
383 Biolabs at 200 MOI for 4 h. Next day, the transfected/transduced fibroblasts were put in co-culture
384 with organoids and submitted to time-lapse imaging. A part of the fibroblasts was further cultured and
385 knockdown/knockout efficiency was determined 72 h after transfection/transduction by qPCR analysis
386 of *Myh9* mRNA levels, normalized to housekeeping genes *Actb* and *Eef1g*, and by immunostaining for
387 MYH9.

388 **LifeAct adenoviral transduction**

389 For imaging experiments with LifeAct, fibroblasts were infected with LifeAct adenoviral particles (IBIDI)
390 according to the manufacturer's instructions prior to co-culture set-up. Briefly, the adenovirus particles
391 were reconstituted in fibroblast cultivation medium at concentration of 500 MOI and incubated with
392 adherent fibroblasts at 37°C for 4 h. After that, adenovirus-containing medium was washed out, and
393 the cells were kept overnight in fibroblast cultivation medium. The next day, GFP fluorescence was
394 checked under the microscope and when > 50% of cells appeared green, fibroblasts were used for co-
395 culture.

396 **Immunofluorescence staining of 2D fibroblasts**

397 For immunofluorescent analysis, fibroblasts were cultured directly on glass coverslips, fixed with 10%
398 neutral buffered formalin, permeabilized with 0.05% Triton X-100 in PBS and blocked with PBS with
399 10% FBS. Then the coverslips were incubated with primary antibodies (Suppl. Table 2) for 2 h at RT or
400 overnight at 4°C. After washing, the coverslips were incubated with secondary antibodies and
401 phalloidin AlexaFluor 488 (Suppl. Table 2) for 2 h at RT. Then the coverslips were washed, stained with
402 DAPI (1 µg/ml; Merck) for 10 min and mounted in Mowiol (Merck). The cells were photographed using
403 Axio Observer Z1 microscope with laser scanning confocal unit LSM 800 with 405, 488, 561 and 640
404 nm lasers, GaAsp PMT detector and objective Plan-Apochromat 40x /1.20 and C-Apochromat 63x /1.20
405 with water immersion (all Zeiss). The brightness of each channel was linearly enhanced in Zen Blue
406 software (Zeiss) and pictures were cropped to final size in Photo Studio 18 (Zoner).

407 **Immunofluorescence staining of 3D co-cultures**

408 For immunofluorescent analysis of 3D co-cultures, the co-cultures were fixed with 10% neutral
409 buffered formalin, washed, and stored in PBS. Next, organoid co-cultures were stained according to
410 the droplet-based method as described (Sumbal and Koledova, 2022). Briefly, the fixed co-cultures
411 were placed on stereoscope (Leica FM165C) and pieces containing an organoid with approximately
412 100 µm of surrounding Matrigel with fibroblasts were manually cut out with 25G needles and moved
413 on parafilm-covered cell culture dish for staining. All the staining steps were done on the parafilm in
414 20 µl drops and all solutions were changed under direct visual control using the stereoscope. The co-
415 cultures were permeabilized with 0.5% Triton X-100 in PBS, blocked with 8% FBS and 0.1% Triton X-
416 100 in PBS (3D staining buffer, 3SB) and incubated with primary antibodies (Suppl. Table 2) in 3SB over
417 1-3 nights at 4°C. Then the co-cultures were washed for 3h with 0.05% Tween-20 in PBS and incubated
418 with secondary antibodies, phalloidin AlexaFluor 488 (Suppl. Table 2) and DAPI (1 µg/ml; Merck) in 3SB
419 over 1-2 nights at 4°C in dark. Then the co-cultures were washed for 3h with 0.05% Tween-20 in PBS,
420 cleared with 60% glycerol and 2.5 M fructose solution overnight at RT in dark and mounted between

421 slide and coverslip with double-sided tape as a spacer. The co-cultures were imaged using inverted
422 microscope Axio Observer 7 with laser scanning confocal unit LSM 880 with 405, 488, 561 and 633 nm
423 lasers, GaAsp PMT spectral detector and objective C-Apochromat 40x /1.20 or C-Apochromat 63x /
424 1.20 with water immersion (all Zeiss). The co-cultures were photographed either as one optical slice
425 or like 3D z-stacks of various z-step as required per experiment. The brightness of each channel was
426 linearly enhanced in Zen Blue software (Zeiss) and pictures were cropped to final size in Photo Studio
427 18 (Zoner). Branch morphometry was manually analyzed from confocal images using ImageJ measure
428 length function, measuring the thickness perpendicular to the long axis of the branch, in the central z-
429 plane.

430 **Image analysis of signal distribution**

431 The analysis of P-ERK intensity and YAP nuclear to cytoplasmic ratio was done in ImageJ (NIH). Cells in
432 optical section in the middle of an organoid branch were manually annotated and segmented for target
433 protein signal (YAP and P-ERK channels) and nuclei (DAPI channel) and density of pixels in YAP and P-
434 ERK channels in the regions of interest (ROIs) was measured. The nuclear to cytoplasmic ratio of YAP
435 was calculated in excel (Microsoft). The spatial information of each ROI was manually measured on a
436 line parallel to the branch longitudinal axis and normalized, with the value "1" set for the tip of the
437 branch and the value "-1" set for the root of the branch. The graphs and linear regression line were
438 created in Prism 6 (GraphPad). Colocalization analysis of YAP and DAPI channels was done in Zen Black
439 (Zeiss) and presented as color-coded (blue DAPI+YAP- and red DAPI+YAP+). The same cut-off for the
440 colocalization analysis was applied for all images from the same experiment.

441 **Real-time quantitative PCR (qPCR)**

442 RNA from fibroblasts was isolated using RNeasy Mini Kit (Qiagen) according to the manufacturer's
443 instruction. RNA concentration was measured using NanoDrop 2000 (Thermo Fisher Scientific). RNA
444 was transcribed into cDNA by using Transcriptor First Strand cDNA Synthesis Kit (Roche) or TaqMan
445 Reverse Transcription kit (Life Technologies). Real-time qPCR was performed using 5 ng cDNA, 5 pmol
446 of the forward and reverse gene-specific primers each (primer sequences are shown in Suppl. Table 3)
447 in Light Cycler SYBR Green I Master mix (Roche) on LightCycler 480 II (Roche). Relative gene expression
448 was calculated using the ΔΔCt method and normalization to two housekeeping genes, β-actin (*Actb*)
449 and eukaryotic elongation factor 1 γ (*Eef1g*).

450 **Transmission electron microscopy**

451 The 3D co-cultures were fixed with 3% glutaraldehyde in 100 mM sodium cacodylate buffer, pH 7.4 for
452 45 min, postfixed in 1% OsO_4 for 50 min, and washed with cacodylate buffer. After embedding in 1%
453 agar blocks, the samples were dehydrated in increasing ethanol series (50, 70, 96, and 100%), treated
454 with 100% acetone, and embedded in Durcupan resin (Merck). Ultrathin sections were prepared using
455 LKB 8802A Ultramicrotome, stained with uranyl acetate and Reynold's lead citrate (Merck), and
456 examined with FEI Morgagni 286(D) transmission electron microscope. The cells in the schematics
457 were segmented manually.

458 **Statistical analysis**

459 Sample size was not determined *a priori* and investigators were not blinded to experimental
460 conditions. Statistical analysis was performed using GraphPad Prism software. Student's t-test
461 (unpaired, two-tailed) was used for comparison of two groups. Bar plots were generated by GraphPad
462 Prism and show mean ± standard deviation (SD). *P < 0.05, **P < 0.01, ***P < 0.001, ****P < 0.0001.
463 The number of independent biological replicates is indicated as n.

Acknowledgements

We are grateful to Danijela Matic Vignjevic for critical review of the manuscript, to Denisa Belisova for mouse husbandry, and to Maria Luisa Martin Faraldo for the LAMA5 antibody. We acknowledge the core facility CELLIM of CEITEC, supported by the Czech-BioImaging large RI project (LM2018129 funded by MEYS CR), for their support with obtaining scientific data presented in this paper. We gratefully acknowledge the Cell and Tissue Imaging Platform (PICT-IBiSA) at Institut Curie, member of the French National Research Infrastructure France-BioImaging (ANR-10-INBS-04). We are thankful to Enantis for providing FGF2-wt. J.S. is supported by Barrande Fellowship (Ministry of Education, Youth and Sports) and FRM FDM202106013570, and by Brno PhD. Talent Scholarship, funded by the Brno City Municipality. This work was supported by grants from the Grant Agency of Masaryk University (MU) (projects no. MUNI/G/1446/2018, MUNI/G/1775/2020 to Z.S.K., MUNI/A/1398/2021 and MUNI/A/1301/2022) and from Internal Grant Agency of Faculty of Medicine MU (MUNI/11/SUP/06/2022 to Z.S.K. and MUNI/IGA/1314/2021 to J.S.).

Author Contributions

Z.S.K. conceptualized the study. J.S. and Z.S.K. designed the experiments. J.S. and Z.S.K. performed all experiments, data analysis, quantification, and statistical analysis. S.F. supervised and funded the experiments performed at Institut Curie. Z.S.K. and J.S. wrote the manuscript. All authors reviewed and edited the manuscript and agreed on its final version.

Conflict of Interest

The authors declare no competing financial interests.

Data availability

The authors declare that all data supporting the findings of this study are available within the article and its supplemental information files or from the corresponding author upon reasonable request.

Limitations of the study

The critical experiment that demonstrates the need of fibroblasts' physical contact with the epithelium for epithelial branching does not allow to distinguish between direct physical contact and potential juxtacrine or very short-distance paracrine signaling between the epithelium and fibroblasts, which may contribute to epithelial morphogenesis.

References

Affolter, M., Zeller, R. and Caussinus, E. (2009). Tissue remodelling through branching morphogenesis. *Nat. Rev. Mol. Cell Biol.* **10**, 831–842.

Barbazan, J., Perez-Gonzalez, C., Gomez-Gonzalez, M., Dedenon, M., Richon, S., Latorre, E., Serra, M., Mariani, P., Descroix, S., Sens, P., et al. (2021). Cancer-associated fibroblasts actively compress cancer cells and modulate mechanotransduction. *bioRxiv* 2021.04.05.438443.

Bonnans, C., Chou, J. and Werb, Z. (2014). Remodelling the extracellular matrix in development and disease. *Nature reviews. Molecular cell biology* **15**, 786.

500 **Brownfield, D. G., Venugopalan, G., Lo, A., Mori, H., Tanner, K., Fletcher, D. A. and Bissell, M. J.**
501 (2013). Patterned collagen fibers orient branching mammary epithelium through distinct
502 signaling modules. *Curr. Biol.* **23**, 703–709.

503 **Conti, M. A., Even-Ram, S., Liu, C., Yamada, K. M. and Adelstein, R. S.** (2004). Defects in cell
504 adhesion and the visceral endoderm following ablation of nonmuscle myosin heavy chain II-A
505 in mice. *J Biol Chem* **279**, 41263–41266.

506 **Costa, A., Kieffer, Y., Scholer-Dahirel, A., Pelon, F., Bourachot, B., Cardon, M., Sirven, P., Magagna,**
507 **I., Fuhrmann, L., Bernard, C., et al.** (2018). Fibroblast Heterogeneity and Immunosuppressive
508 Environment in Human Breast Cancer. *Cancer Cell* **33**, 463-479.e10.

509 **Ender, P., Gagliardi, P. A., Dobrzyński, M., Frismantiene, A., Dessauges, C., Höhener, T., Jacques,**
510 **M.-A., Cohen, A. R. and Pertz, O.** (2022). Spatiotemporal control of ERK pulse frequency
511 coordinates fate decisions during mammary acinar morphogenesis. *Developmental Cell*
512 S1534580722005949.

513 **Ewald, A. J., Brenot, A., Duong, M., Chan, B. S. and Werb, Z.** (2008). Collective epithelial migration
514 and cell rearrangements drive mammary branching morphogenesis. *Dev. Cell* **14**, 570–581.

515 **Fata, J. E., Werb, Z. and Bissell, M. J.** (2004). Regulation of mammary gland branching
516 morphogenesis by the extracellular matrix and its remodeling enzymes. *Breast Cancer Res* **6**,
517 1–11.

518 **Feinberg, T. Y., Zheng, H., Liu, R., Wicha, M. S., Yu, S. M. and Weiss, S. J.** (2018). Divergent Matrix-
519 Remodeling Strategies Distinguish Developmental from Neoplastic Mammary Epithelial Cell
520 Invasion Programs. *Dev. Cell* **47**, 145-160.e6.

521 **Goodwin, K. and Nelson, C. M.** (2020). Branching morphogenesis. *Development* **147**, dev184499.

522 **Goodwin, K., Mao, S., Guyomar, T., Miller, E., Radisky, D. C., Košmrlj, A. and Nelson, C. M.** (2019).
523 Smooth muscle differentiation shapes domain branches during mouse lung development.
524 *Development* **146**,.

525 **Hammer, A. M., Sizemore, G. M., Shukla, V. C., Avendano, A., Sizemore, S. T., Chang, J. J., Kladney,**
526 **R. D., Cuitiño, M. C., Thies, K. A., Verfurth, Q., et al.** (2017). Stromal PDGFR-α Activation
527 Enhances Matrix Stiffness, Impedes Mammary Ductal Development, and Accelerates Tumor
528 Growth. *Neoplasia* **19**, 496–508.

529 **Heisenberg, C.-P. and Bellaïche, Y.** (2013). Forces in tissue morphogenesis and patterning. *Cell* **153**,
530 948–962.

531 **Hino, N., Rossetti, L., Marín-Llauradó, A., Aoki, K., Trepat, X., Matsuda, M. and Hirashima, T.** (2020).
532 ERK-Mediated Mechanochemical Waves Direct Collective Cell Polarization. *Developmental*
533 *Cell* **53**, 646-660.e8.

534 **Hirashima, T. and Matsuda, M.** (2021). *ERK-mediated Curvature Feedback Regulates Branching*
535 *Morphogenesis in Lung Epithelial Tissue*.

536 **Huebner, R. J., Lechler, T. and Ewald, A. J.** (2014). Developmental stratification of the mammary
537 epithelium occurs through symmetry-breaking vertical divisions of apically positioned luminal
538 cells. *Development* **141**, 1085–1094.

539 **Huebner, R. J., Neumann, N. M. and Ewald, A. J.** (2016). Mammary epithelial tubes elongate through
540 MAPK-dependent coordination of cell migration. *Development* **143**, 983–993.

541 **Hughes, A. J., Miyazaki, H., Coyle, M. C., Zhang, J., Laurie, M. T., Chu, D., Vavrušová, Z., Schneider,**
542 **R. A., Klein, O. D. and Gartner, Z. J.** (2018). Engineered Tissue Folding by Mechanical
543 Compaction of the Mesenchyme. *Dev. Cell* **44**, 165-178.e6.

544 **Jones, C. E., Hammer, A. M., Cho, Y., Sizemore, G. M., Cukierman, E., Yee, L. D., Ghadiali, S. N.,**
545 **Ostrowski, M. C. and Leight, J. L.** (2019). Stromal PTEN Regulates Extracellular Matrix
546 Organization in the Mammary Gland. *Neoplasia* **21**, 132–145.

547 **Kim, H. Y., Pang, M.-F., Varner, V. D., Kojima, L., Miller, E., Radisky, D. C. and Nelson, C. M.** (2015).
548 Localized Smooth Muscle Differentiation Is Essential for Epithelial Bifurcation during
549 Branching Morphogenesis of the Mammalian Lung. *Dev. Cell* **34**, 719–726.

550 **Koledova, Z.** (2017). 3D Coculture of Mammary Organoids with Fibrospheres: A Model for Studying
551 Epithelial-Stromal Interactions During Mammary Branching Morphogenesis. *Methods Mol.*
552 *Biol.* **1612**, 107–124.

553 **Koledova, Z. and Lu, P.** (2017). A 3D Fibroblast-Epithelium Co-culture Model for Understanding
554 Microenvironmental Role in Branching Morphogenesis of the Mammary Gland. *Methods*
555 *Mol. Biol.* **1501**, 217–231.

556 **Koledova, Z., Zhang, X., Streuli, C., Clarke, R. B., Klein, O. D., Werb, Z. and Lu, P.** (2016). SPRY1
557 regulates mammary epithelial morphogenesis by modulating EGFR-dependent stromal
558 paracrine signaling and ECM remodeling. *Proc. Natl. Acad. Sci. U.S.A.* **113**, E5731-5740.

559 **Kouros-Mehr, H. and Werb, Z.** (2006). Candidate regulators of mammary branching morphogenesis
560 identified by genome-wide transcript analysis. *Dev. Dyn.* **235**, 3404–3412.

561 **Labernadie, A., Kato, T., Brugués, A., Serra-Picamal, X., Derzsi, S., Arwert, E., Weston, A., González-**
562 **Tarragó, V., Elosegui-Artola, A., Albertazzi, L., et al.** (2017). A mechanically active
563 heterotypic E-cadherin/N-cadherin adhesion enables fibroblasts to drive cancer cell invasion.
564 *Nat. Cell Biol.* **19**, 224–237.

565 **Li, R., Bernau, K., Sandbo, N., Gu, J., Preissl, S. and Sun, X.** (2018). Pdgfra marks a cellular lineage
566 with distinct contributions to myofibroblasts in lung maturation and injury response. *eLife* **7**,
567 e36865.

568 **Li, R., Li, X., Hagood, J., Zhu, M.-S. and Sun, X.** (2020a). Myofibroblast contraction is essential for
569 generating and regenerating the gas-exchange surface. *J Clin Invest* **130**, 2859–2871.

570 **Li, C. M.-C., Shapiro, H., Tsiobikas, C., Selfors, L. M., Chen, H., Rosenbluth, J., Moore, K., Gupta, K.**
571 **P., Gray, G. K., Oren, Y., et al.** (2020b). Aging-Associated Alterations in Mammary Epithelia
572 and Stroma Revealed by Single-Cell RNA Sequencing. *Cell Rep* **33**, 108566.

Muzumdar, M. D., Tasic, B., Miyamichi, K., Li, L. and Luo, L. (2007). A global double-fluorescent Cre reporter mouse. *Genesis* **45**, 593–605.

Nerger, B. A., Jaslove, J. M., Elashal, H. E., Mao, S., Košmrlj, A., Link, A. J. and Nelson, C. M. (2021). Local accumulation of extracellular matrix regulates global morphogenetic patterning in the developing mammary gland. *Current Biology*.

Nguyen-Ngoc, K.-V. and Ewald, A. J. (2013). Mammary ductal elongation and myoepithelial migration are regulated by the composition of the extracellular matrix. *J Microsc* **251**, 212–223.

Palmer, M. A., Nerger, B. A., Goodwin, K., Sudhakar, A., Lemke, S. B., Ravindran, P. T., Toettcher, J. E., Košmrlj, A. and Nelson, C. M. (2021). Stress ball morphogenesis: How the lizard builds its lung. *Science Advances*.

Panciera, T., Azzolin, L., Cordenonsi, M. and Piccolo, S. (2017). Mechanobiology of YAP and TAZ in physiology and disease. *Nat Rev Mol Cell Biol* **18**, 758–770.

Pérez-González, C., Ceada, G., Greco, F., Matejčić, M., Gómez-González, M., Castro, N., Menendez, A., Kale, S., Krndija, D., Clark, A. G., et al. (2021). Mechanical compartmentalization of the intestinal organoid enables crypt folding and collective cell migration. *Nat Cell Biol* **23**, 745–757.

Peuhu, E., Kaukonen, R., Lerche, M., Saari, M., Guzmán, C., Rantakari, P., De Franceschi, N., Wärri, A., Georgiadou, M., Jacquemet, G., et al. (2017). SHARPIN regulates collagen architecture and ductal outgrowth in the developing mouse mammary gland. *EMBO J.* **36**, 165–182.

Riedl, J., Flynn, K. C., Raducanu, A., Gärtner, F., Beck, G., Bösl, M., Bradke, F., Massberg, S., Aszodi, A., Sixt, M., et al. (2010). Lifeact mice for studying F-actin dynamics. *Nat Methods* **7**, 168–169.

Sahai, E., Astsaturov, I., Cukierman, E., DeNardo, D. G., Egeblad, M., Evans, R. M., Fearon, D., Greten, F. R., Hingorani, S. R., Hunter, T., et al. (2020). A framework for advancing our understanding of cancer-associated fibroblasts. *Nature Reviews Cancer* **20**, 174–186.

Shyer, A. E., Tallinen, T., Nerurkar, N. L., Wei, Z., Gil, E. S., Kaplan, D. L., Tabin, C. J. and Mahadevan, L. (2013). Villification: how the gut gets its villi. *Science* **342**, 212–218.

Shyer, A. E., Rodrigues, A. R., Schroeder, G. G., Kassianidou, E., Kumar, S. and Harland, R. M. (2017). Emergent cellular self-organization and mechanosensation initiate follicle pattern in the avian skin. *Science* **357**, 811–815.

Silberstein, G. B. and Daniel, C. W. (1982). Glycosaminoglycans in the basal lamina and extracellular matrix of the developing mouse mammary duct. *Dev Biol* **90**, 215–222.

Sirka, O. K., Shamir, E. R. and Ewald, A. J. (2018). Myoepithelial cells are a dynamic barrier to epithelial dissemination. *J Cell Biol* **217**, 3368–3381.

608 **Sternlicht, M. D., Sunnarborg, S. W., Kouros-Mehr, H., Yu, Y., Lee, D. C. and Werb, Z.** (2005).
609 Mammary ductal morphogenesis requires paracrine activation of stromal EGFR via ADAM17-
610 dependent shedding of epithelial amphiregulin. *Development* **132**, 3923–3933.

611 **Sumbal, J. and Koledova, Z.** (2019). FGF signaling in mammary gland fibroblasts regulates multiple
612 fibroblast functions and mammary epithelial morphogenesis. *Development* **146**,.

613 **Sumbal, J. and Koledova, Z.** (2022). Single Organoids Droplet-Based Staining Method for High-End 3D
614 Imaging of Mammary Organoids. *Methods Mol Biol* **2471**, 259–269.

615 **Sumbal, J., Belisova, D. and Koledova, Z.** (2020). Fibroblasts: The grey eminence of mammary gland
616 development. *Semin Cell Dev Biol*.

617 **Wang, S., Sekiguchi, R., Daley, W. P. and Yamada, K. M.** (2017). Patterned cell and matrix dynamics
618 in branching morphogenesis. *Journal of Cell Biology* **216**, 559–570.

619 **Wendling, O., Bornert, J.-M., Chambon, P. and Metzger, D.** (2009). Efficient temporally-controlled
620 targeted mutagenesis in smooth muscle cells of the adult mouse. *genesis* **47**, 14–18.

621 **Wiseman, B. S. and Werb, Z.** (2002). Stromal effects on mammary gland development and breast
622 cancer. *Science* **296**, 1046–1049.

623 **Yoshitake, R., Chang, G., Saeki, K., Ha, D., Wu, X., Wang, J. and Chen, S.** (2022). Single-Cell
624 Transcriptomics Identifies Heterogeneity of Mouse Mammary Gland Fibroblasts With Distinct
625 Functions, Estrogen Responses, Differentiation Processes, and Crosstalks With Epithelium.
626 *Front Cell Dev Biol* **10**, 850568.

627 **Zhao, C., Cai, S., Shin, K., Lim, A., Kalisky, T., Lu, W.-J., Clarke, M. F. and Beachy, P. A.** (2017).
628 Stromal Gli2 activity coordinates a niche signaling program for mammary epithelial stem
629 cells. *Science* **356**,.

630

Figures

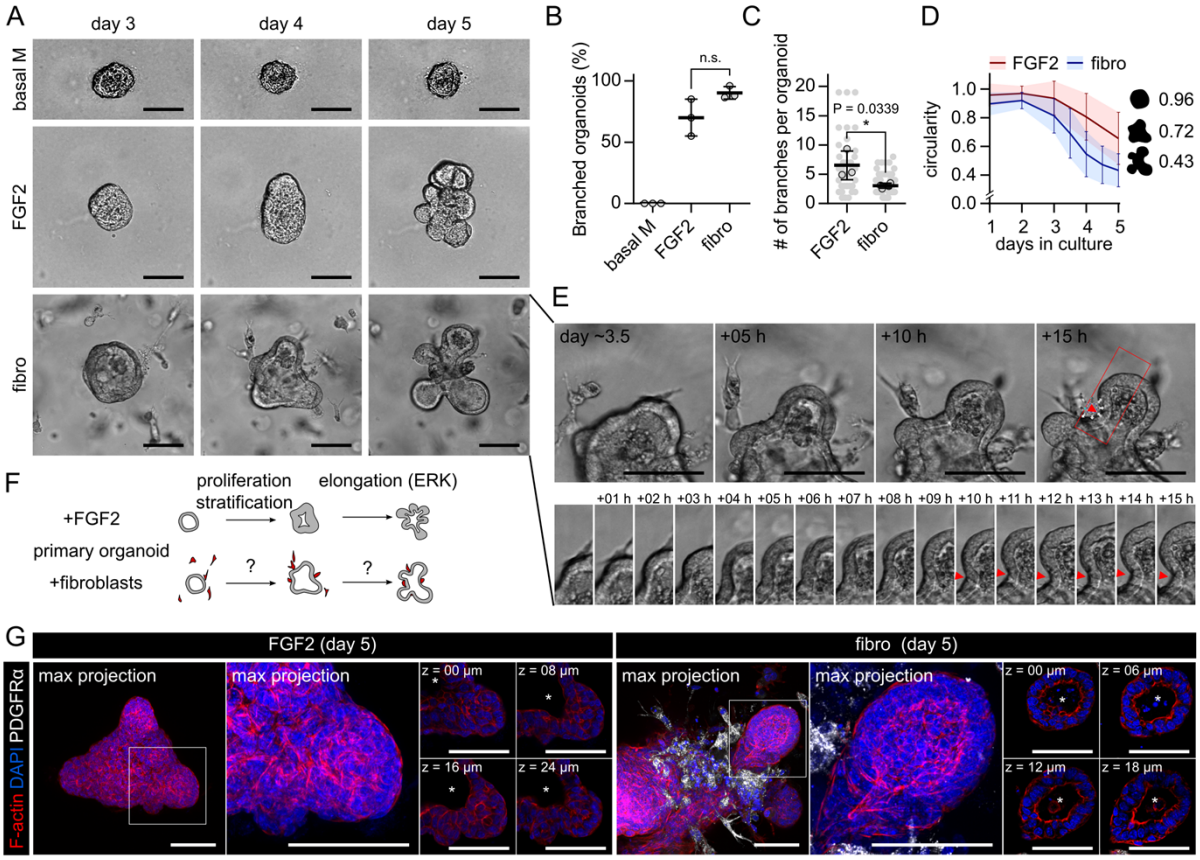

Figure 1. Fibroblast-induced branching of organoids does not reproduce FGF2-induced budding. A. Snapshots from time-lapse imaging of primary mammary organoids in basal organoid medium (basal M) without any FGF supplementation (top), basal M with FGF2 (middle), or co-cultured with primary mammary fibroblasts (fibro) in basal M with no FGF supplementation (bottom). Scale bar: 100 µm. Full videos are presented in Suppl. Video 1. **B.** Quantification of percentage of branched organoids per all organoids in the conditions from **A**. The plot shows mean ± SD, each dot represents biologically independent experiment, n = 3. Statistical analysis: Two-tailored *t*-test. **C.** Quantification of number of branches per branched organoids in conditions from **A**. The plot shows mean ± SD, each lined dot shows mean from each experiment, each faint dot shows single organoid measurement, n = 3 biologically independent experiments, N = 20 organoids per experiment. Statistical analysis: Two-tailored *t*-test. **D.** Quantification of organoid circularity in conditions from **A**, the lines represent mean, the shadows and error bars represent ± SD, n = 3 biologically independent experiments, N = 20 organoids per experiment. The schemes show representative shape of given circularity. **E.** Detailed images of branch development in co-culture with fibroblasts from **A**. Scale bar: 20 µm. **F.** A scheme depicting differences between organoid budding induced by exogenous FGF2 and organoid branching in co-culture with fibroblasts. **G.** Maximum intensity projection of F-actin (red), DAPI (blue) and PDGFRα (white) in organoid with exogenous FGF2 or with fibroblasts (fibro). Zoom-in area from the box is depicted as maximum projection and single z slices. Scale bar: 100 µm.

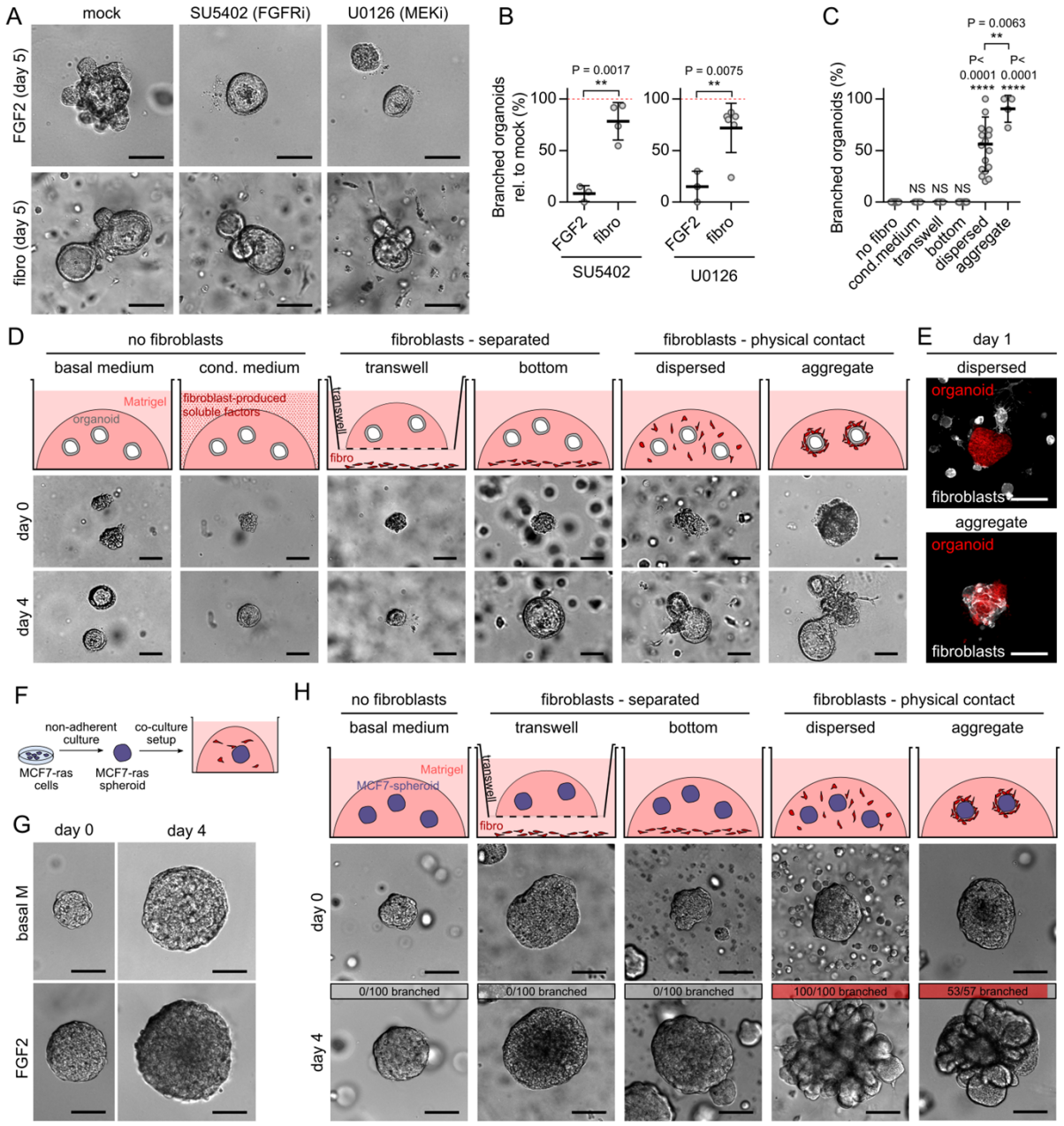

Figure 2. Endogenous paracrine signals are not sufficient to induce organoid branching. A. Representative organoids cultured with exogenous FGF2 or with fibroblasts (fibro), treated with inhibitor of FGFR (SU5402) and MEK (U0126). Scale bar: 100 µm. **B.** Quantification of branched organoid per all organoids, relative to mock. The plots show mean ± SD, each dot represents biologically independent experiment, n = 3-5, N = 20 organoids per experiment. Statistical analysis: Two-tailored *t*-test. **C.** Quantification of organoid branching in different co-culture set-ups. The plot shows mean ± SD, each dot represents biologically independent experiment, n = 16 independent experiments for "no fibro", 5 for "cond. medium", 5 for "transwell", 12 for "bottom", 16 for "dispersed", and 4 for "aggregate", N = 20 organoids per experiment. Statistical analysis: Multiple *t*-tests compared to control "no fibro", or indicated by the line. **D.** Schemes and images on day 0 and day 4 of different organoid-fibroblast co-culture set-ups. Scale bar: 100 µm. **E.** Dispersed and aggregated co-culture of LifeAct-GFP fibroblast (white) and tdTomato organoid (red) at the beginning of the culture. Scale bar: 100 µm. **F.** A scheme of MCF7-ras spheroid co-culture setup. **G.** Representative MCF7-ras spheroid cultured in basal organoid medium (basal M) or basal M with

666 exogenous FGF2. Scale bar: 100 µm. **H.** Schemes and images on day 0 and day 4 of different spheroid-
667 fibroblast co-culture set-ups. Top grey and red bars indicate proportion of branched spheroids out of
668 all spheroids per condition, n = 3-5 independent experiment, N = 20 spheroids per experiment. Scale
669 bar: 100 µm.

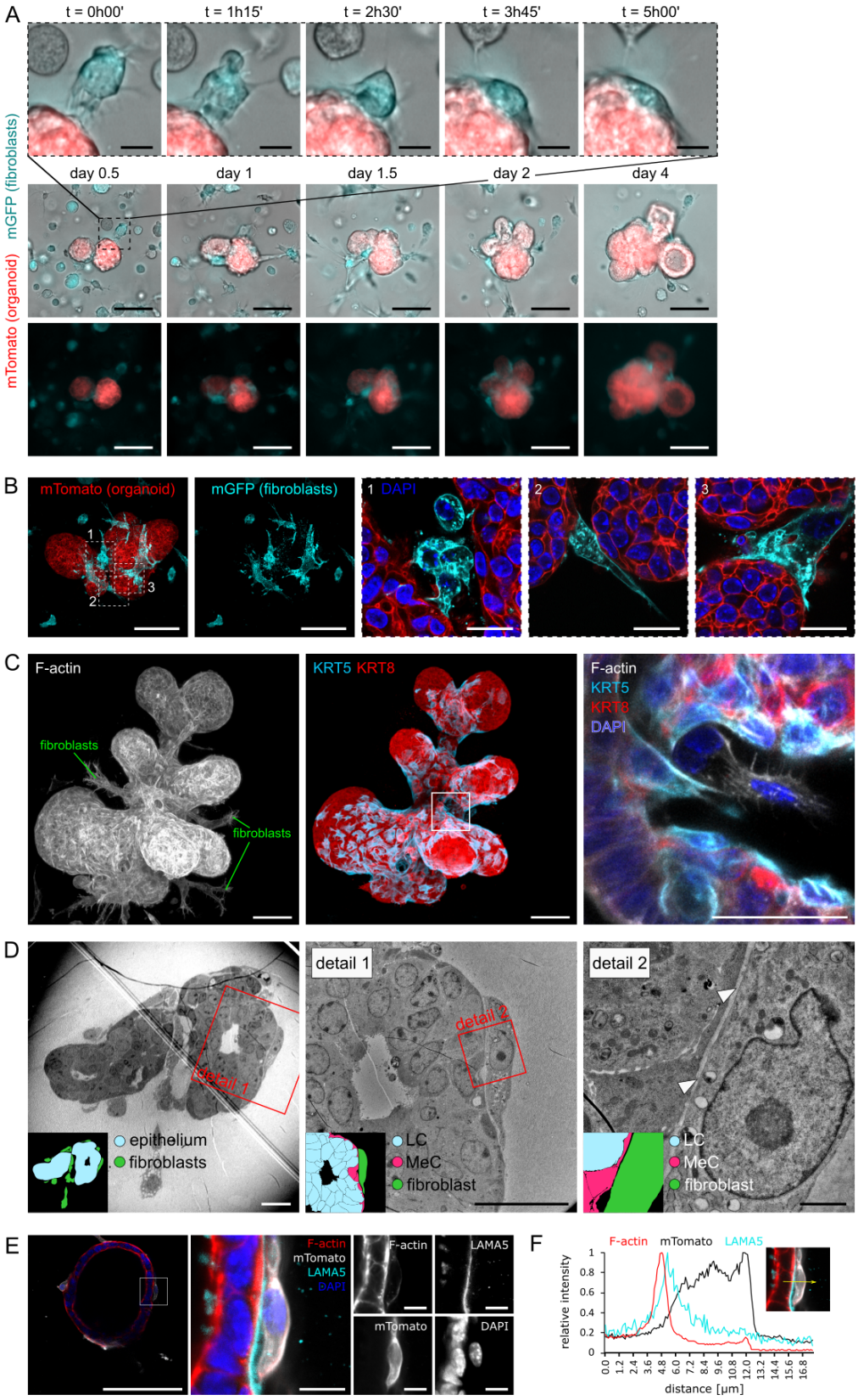

Figure 3. Fibroblasts in co-cultures are in physical contact with the epithelium. A. Snapshots from time-lapse brightfield and fluorescence imaging of organoid (tdTomato) and fibroblast (GFP) co-culture. Scale bar: 100 µm. Top line shows detail of fibroblast-organoid close interaction. Scale bar: 20 µm. **B.** Images of the contact point between organoid (tdTomato) and fibroblasts (GFP) on day 4 of co-

culture. Scale bar: 100 µm, scale bar in detail: 20 µm. **C.** Images of the contact point between luminal (KRT8) and basal (KRT5) epithelial cells and fibroblasts (F-actin) on day 4 of co-culture. Scale bar: 20 µm, scale bar in detail: 10 µm. Video projection of the fibroblast-branched organoid is presented in Suppl. Video 3. **D.** Transmission electron micrographs and scheme (inset) of the contact point between luminal (LC, blue) and myoepithelial (MeC, magenta) cells and fibroblasts (green) on day 4 of co-culture. Scale bar: 20 µm, scale bar in detail: 2 µm. **E.** Optical slice of organoid-fibroblast co-culture, laminin 5 (cyan), DAPI (blue), F-actin (red), fibroblasts were isolated from *R26-mT/mG* mice (mTomato, white). Scale bar: 100 µm, scale bar in detail: 10 µm. **F.** A representative 1D relative fluorescence intensity plot. The measurement line is depicted in yellow (right).

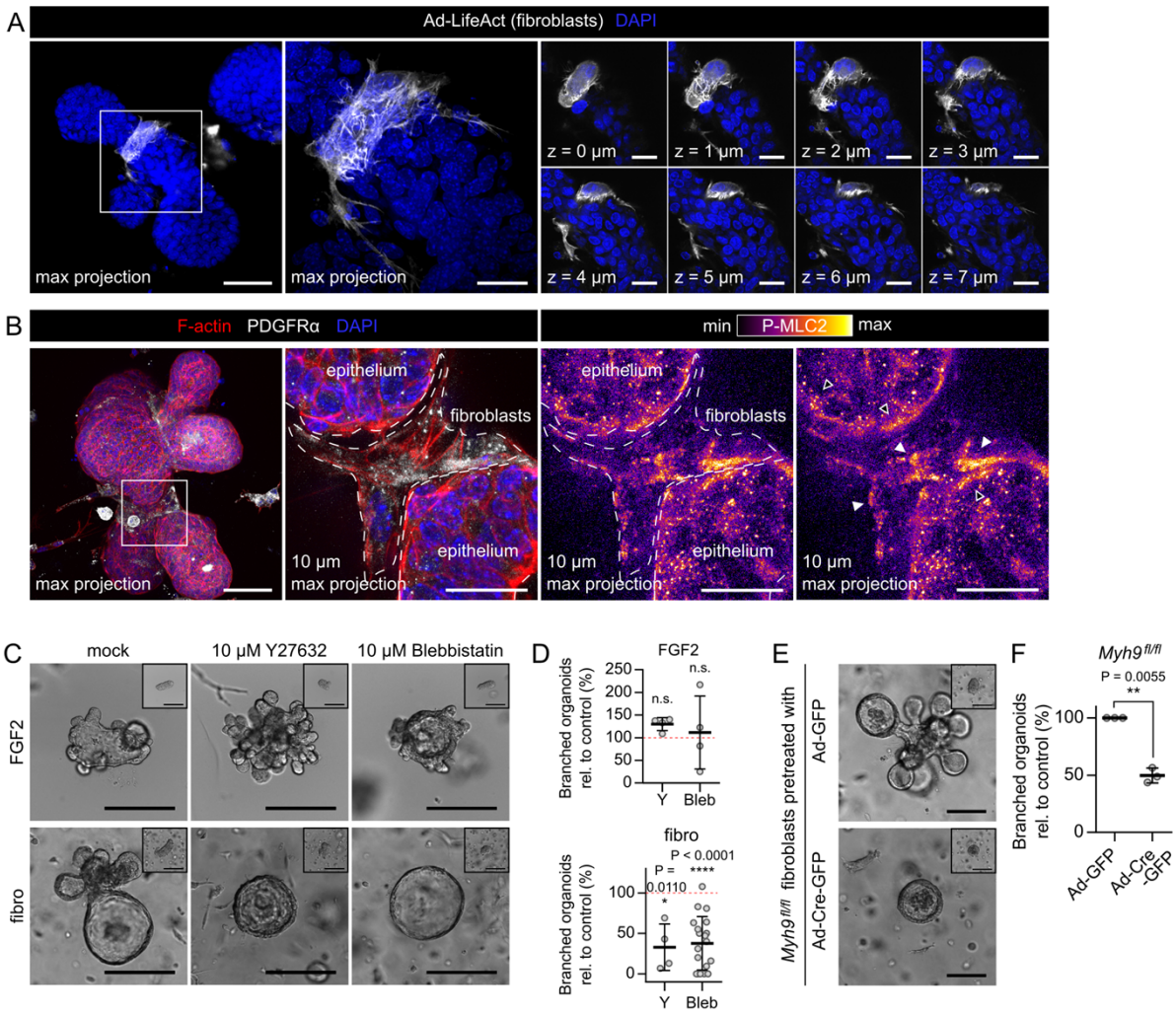

Figure 4. Fibroblast-induced branching requires fibroblast contractility. A. Maximum projection (left), detailed maximum projection (middle) and detail optical sections (right) of organoid branch induced in co-culture with fibroblasts (day 4). DAPI (blue), fibroblasts prelabeled with Ad-LifeAct-GFP (white). Scale bar: 50 µm, scale bar in detail: 20 µm. **B.** Full maximum projection (left) and 10 µm maximum projection (both middle and right) of organoid co-cultured with fibroblasts. F-actin (red), PDGFRα (white), DAPI (blue) and phosphorylated myosin light chain 2 (P-MLC2, fire LUT). Scale bar: 50 µm, scale bar in detail: 20 µm. **C.** Images of organoids on day 5 of culture (with day 0 insets) with FGF2 or with fibroblasts and treated with mock (DMSO) or contraction inhibitors (ROCK1/2 inhibitor Y27632 or non-muscle myosin II inhibitor blebbistatin). Scale bar: 100 µm. **D.** The plots show organoid branching with contraction inhibitors as mean ± SD. Statistical analysis: Multiple *t*-tests between each treatment and the mock-treated control; n = 4-18 (each dot represents a biologically independent experiment), N = 20 organoids per experiment. **E.** Images of organoids on day 5 of culture (with day 0 insets) co-cultured with control or *Myh9* knock-out fibroblasts. Scale bar: 100 µm. Videos from the 5-day experiment are presented in Suppl. Video 5. **F.** The plot shows organoid branching with mean ± SD. Statistical analysis: two-tailored paired *t*-test; n = 3 (each dot represents a biologically independent experiment), N = 20 organoids per experiment.

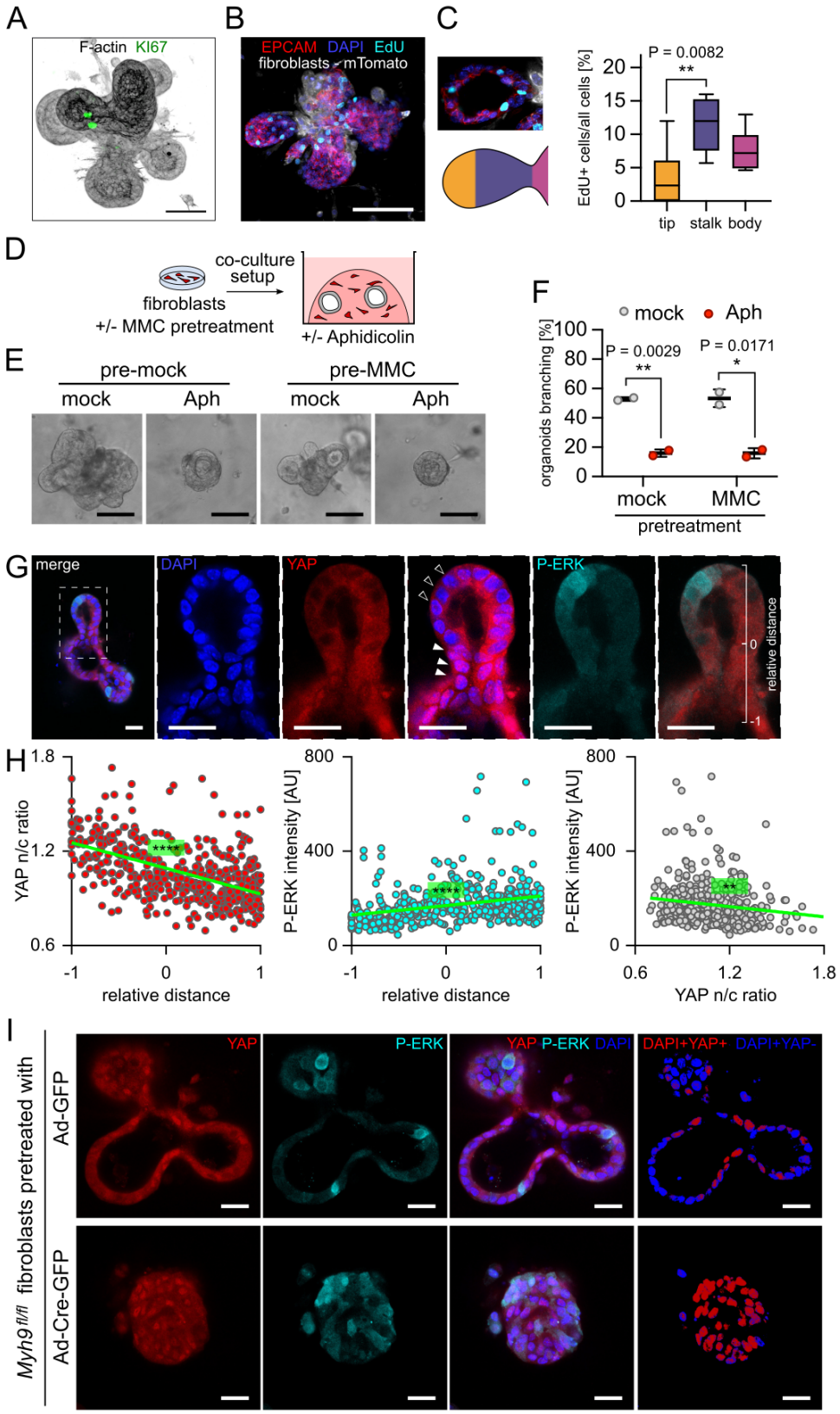

701

702 **Figure 5. Epithelial mechanisms required for fibroblast-induced branching. A.** F-actin (black) and KI67
703 (green) staining in organoids cultured with fibroblasts, day 4 of culture. Scale bar: 50 µm. The panel is
704 related to Suppl. Figure 5A. **B.** Organoid on day 4 of co-culture, EdU administered 2 h pre-fix, EPCAM
705 (red), DAPI (blue), EdU (cyan), fibroblasts were isolated from *R26-mT/mG* mice (mTomato, white).

706 Scale bar: 100 µm. The panel is related to Suppl. Figure 5B. **C.** Optical section of a branch from **B** (top),
707 a scheme of branch regions (bottom), and quantification of percentage of EdU+ cells from all cells in
708 different branch regions. The box and whiskers plot shows minimum, median, and maximum values,
709 and second and third quartiles of data distribution. Statistical analysis: Multiple *t*-tests. **D.** A scheme of
710 the proliferation-inhibition experiment. **E.** Co-cultures at day 5, fibroblasts pretreated with +/-
711 mitomycin C (MMC), co-cultures treated with +/- aphidicolin (Aph). Scale bar: 100 µm. **F.** Quantification
712 of the percentage of branched organoids from experiment in **E**. The plot shows mean ± SD, each dot
713 represent biologically independent experiment, n = 2, N = 51-77 organoids per sample, statistical
714 analysis: *t*-test. **G.** Staining of YAP and phosphorylated ERK (P-ERK) in an organoid co-cultured with
715 fibroblasts. Scale bar: 20 µm. **H.** Quantification of YAP nuclear/cytoplasmic signal ratio and P-ERK signal
716 intensity. Relative distance -1 is branch root, +1 is branch tip. Each dot represents a single cell, n = 436
717 cells from 19 branches of 10 organoids. Statistical analysis: Linear regression. **I.** Staining of YAP and
718 phosphorylated ERK (P-ERK) in organoids co-cultured with control or *Myh9* knock-out fibroblasts. Scale
719 bar: 200 µm.